Current Applied Physics 18 (2018) 114–121

Contents lists available at ScienceDirect

Current Applied Physics

journal homepage: www.elsevier.com/locate/cap

# Uniaxial deformation of nanotwinned nanotubes in body-centered cubic tungsten

Shuozhi Xu [a, *], Saeed Zare Chavoshi [b]

[a] California NanoSystems Institute, University of California, Santa Barbara, Santa Barbara, CA, 93106-6105, USA
[b] Department of Mechanical Engineering, Imperial College London, London, SW7 2AZ, UK

ARTICLE INFO

*Article history:*
Received 21 July 2017
Received in revised form
26 September 2017
Accepted 5 October 2017
Available online 7 October 2017

*Keywords:*
Nanotwinned nanotube
Metallic materials
Molecular dynamics
Plastic deformation

ABSTRACT

We perform large-scale molecular dynamics simulations to delve into tensile and compressive loading of nanotubes containing {112} nanoscale twins in body-centered cubic tungsten, as a function of wall thickness, twin boundary spacing, and strain rate. Solid nanopillars without the interior hollow and/or nanotubes without the nanoscale twins are also investigated as references. Our findings demonstrate that both stress-strain response and deformation behavior of nanotwinned nanotubes and nanopillars exhibit a strong tension-compression asymmetry. The yielding of the nanotwinned nanotubes with thick walls is governed by dislocation nucleation from the twin boundary/surface intersections. With a small wall thickness, however, the failure of the nanotwinned nanotubes is dominated by crack formation and buckling under tensile and compressive loading, respectively. In addition, the strain rate effect, which is more pronounced in compressive loading than in tensile loading, increases with a decreasing twin boundary spacing.



## 1. Introduction

Metallic nanopillars exhibit a higher strength as their cross section areas decrease [1], a feature attributed to the existence of exterior free surfaces. Following the idea of carbon nanotubes, which have extraordinary mechanical and thermal properties [2], a new category of metallic nanopillars, namely metallic nanotubes, have recently been created by introducing interior hollow along the pillar central axis [3]. Besides the outer diameter, nanotubes have an additional feature size, i.e., the wall thickness, as compared to the corresponding solid nanopillars. To the best of our knowledge, all molecular dynamics (MD) studies of the metallic nanotubes so far are in face-centered cubic (FCC) systems, including Cu [4–7], Au [3,4,8], and Ni [9]. The MD simulations of Sun et al. [3] established that the tensile yield strength in [111] Au nanotubes is up to 60% higher than that of the corresponding nanopillar, owing to the repulsive image force exerted by the interior surface against dislocation nucleation from the outer surface. Ji and Park [7] discovered that, with the Mishin embedded-atom method (EAM) potential [10], the Young's modulus of the Cu nanotubes along a ⟨100⟩ axial direction decreases with a decreasing wall thickness $t$. Nevertheless, opposite results that the Young's modulus of the same nanotubes negatively correlates with $t$ were reported by Zhang et al. [6] when the Doyama-Kogure EAM potential [11] was employed. Zhang et al. [6] also found that while a tensile residual stress is obtained at the outer surface of the nanotubes (as in the case of the nanopillars), either a tensile or a compressive stress status can be achieved at the inner surface depending on the wall thickness. Meanwhile, Cao et al. [8] argued that in Au, ultrahigh plastic flow stress of more than 2 GPa could be maintained at up to

* Corresponding author.
*E-mail address:* shuozhixu@ucsb.edu (S. Xu).

https://doi.org/10.1016/j.cap.2017.10.003
1567-1739/

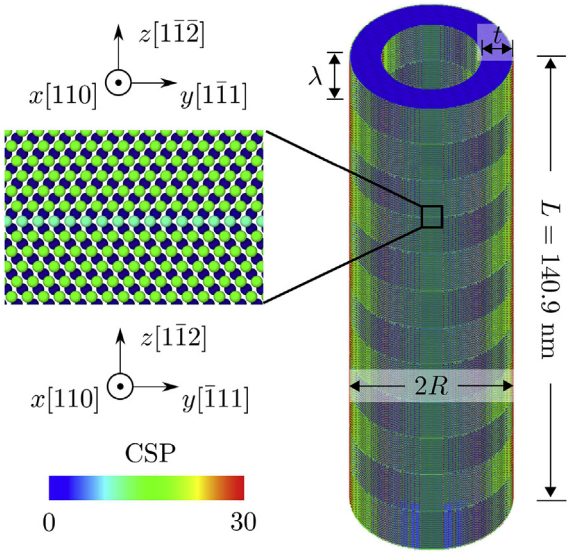


**Fig. 1.** Atomic structure of a nanotwinned nanotube with an outer radius $R = 20$ nm, wall thickness $t$, and TB spacing $\lambda$. A close-up view of the TB is also presented. Atoms are colored by CSP [27].

60% and 5% tensile strain in nanotubes and solid nanopillars, respectively. Other MD simulations [5,7,8] also confirmed a universal trend of surface reconstruction to the energetically favorable close-packed {111} orientation in FCC nanotubes regardless of the initial crystallographic orientation, which may be responsible for the ultrahigh plasticity in the nanotubes.

In addition to the interior surface [12–14], the mechanical properties of the nanopillars/nanotubes can also be altered by introducing nanoscale twins. A new feature size, twin boundary (TB) spacing, thus emerges. In Au nanopillars, a critical ratio of the pillar diameter $D$ to the TB spacing $\lambda$ exists corresponding to a transition from strain hardening to softening [15], as well as one from TB-induced strengthening to softening [16]. For Cu nanopillars, there is an optimal length-to-diameter aspect ratio for which the twinned nanopillars always have a higher yield stress than their twin-free counterparts [17]. There are also implications that the nanotwinned Cu nanopillars with a square cross section exhibit a stronger strengthening effect due to the existence of twins than those with a circular one [18].

Despite numerous MD studies of nanotubes and nanotwinned nanopillars, respectively, we are not aware of any investigation of nanopillars that contain both interior hollow and nanoscale twins, i.e., nanotwinned nanotubes. Thus, it remains to be seen how the two feature sizes — wall thickness and TB spacing — affect the

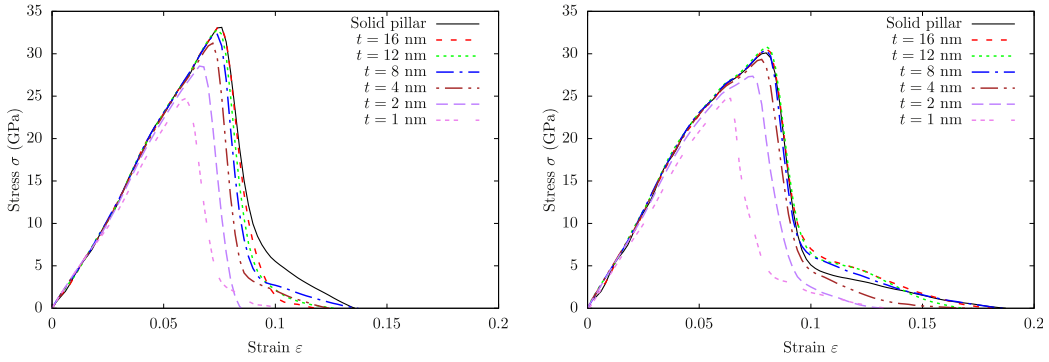


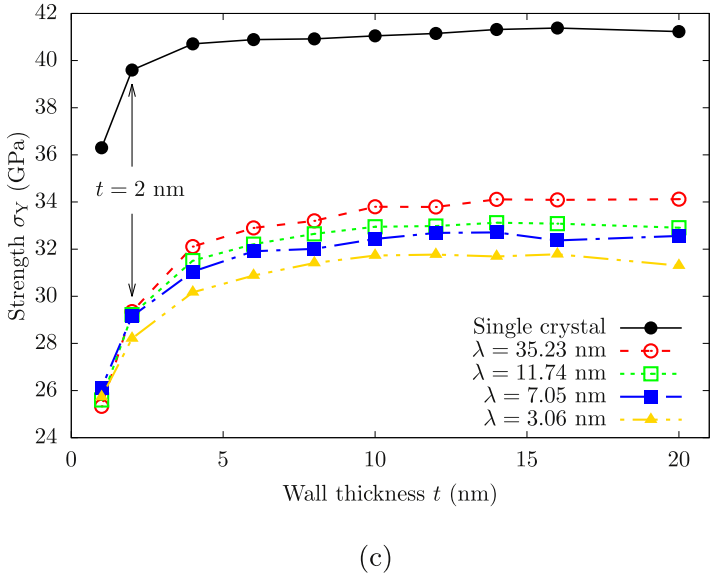


**Fig. 2.** Stress-strain curves of nanotwinned nanotubes under tensile loading with different wall thickness $t$ when TB spacing (a) $\lambda = 35.23$ nm and (b) $\lambda = 3.06$ nm. The strength $\sigma_Y$ as a function of $t$ and $\lambda$ is given in (c). Note that the cases of solid nanopillars ($t = R = 20$ nm) and single crystalline nanotubes are also presented as references.

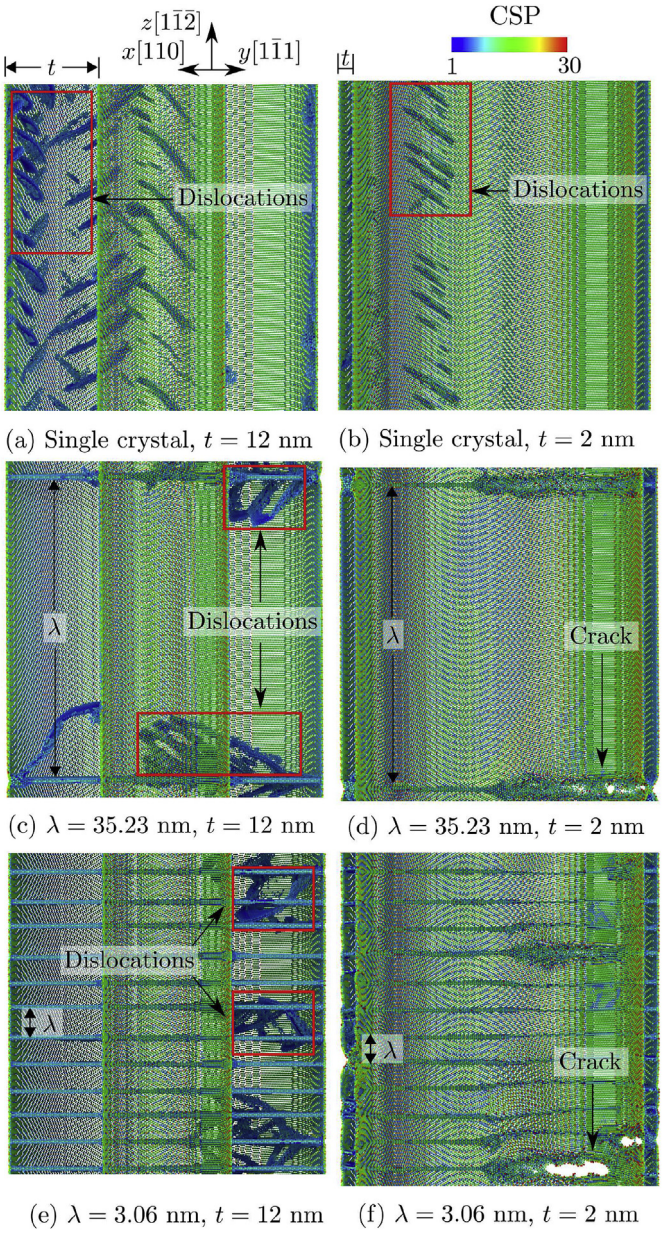


**Fig. 3.** Under tensile loading, snapshots of atomic structures on the threshold of yielding/failure in single crystalline nanotubes with wall thickness (a) $t = 12$ nm and (b) $t = 2$ nm, nanotwinned nanotubes ($\lambda = 35.12$ nm) with (c) $t = 12$ nm and (d) $t = 2$ nm, as well as nanotwinned nanotubes ($\lambda = 3.06$ nm) with (e) $t = 12$ nm and (f) $t = 2$ nm. Atoms are colored by CSP [27]; those with a CSP smaller than 1 are removed.

mechanical properties of nanopillars, which will assist in enhancing our understanding of physical response of these material systems. Furthermore, as mentioned earlier, compared with FCC systems, nanopillars in body-centered cubic (BCC) metals are much less investigated. Most studies of the BCC systems (with the exceptions of Refs. [19,20]) do not consider preexisting nanoscale twins, since their high stacking fault energy makes it difficult to generate nanoscale twins by growth method. These facts certainly point to the need for further MD studies specifically addressing the role of wall thickness and TB spacing on mechanical behavior of nanotwinned nanotubes in BCC metals. Thus, in this paper, we focus on exploring the deformation of nanotwinned nanotubes in BCC tungsten (W) subject to tensile and compressive loading: three parameters — wall thickness, TB spacing, and strain rate — will be varied independently to assess their influences.

## 2. Methods

MD simulations are performed using LAMMPS [21]. The EAM potential of Marinica et al. [22] is employed to describe the interatomic interactions in W because, based on density functional theory calculations, this potential well reproduces the dislocation core structure, Peierls potential, kink-pair energy, and generalized stacking fault energy [23]. As the validity of MD simulation results significantly hinges on the choice of interatomic potential, it is particularly important to adopt a suitable potential for BCC metals because few accurate ones exist [24–26]. All nanotubes have the same initial length $L = 140.9$ nm and a circular cross section with an outer radius $R = 20$ nm, as shown in Fig. 1. A wall thickness $t$ ranging from 1 nm to 16 nm and a uniform {112} TB spacing $\lambda$ varying from 3.06 nm to 35.23 nm are employed. Periodic boundary conditions are applied along the ⟨112⟩ central axis, while other boundaries are assumed traction-free. Solid nanopillars (i.e., $t = R = 20$ nm) with the same $L$ and $\lambda$ are also studied for comparison. In all single crystals, the lattice orientations are $x[110]$, $y[1\bar{1}1]$, and $z[1\bar{1}\bar{2}]$. With a lattice parameter $a_0 = 3.14339$ Å, the simulation cells used in this paper contain about 1.1 million (nanotube with $t = 1$ nm) to about 11.4 million (solid nanopillar) atoms.

Each nanotube/nanopillar was first dynamically relaxed at 10 K for 20 ps under an isobaric zero-stress condition, followed by an energy minimization using the conjugate gradient method; then a homogeneous deformation at a constant engineering strain rate of $\pm 10^9$ s$^{-1}$ is applied along the $z$ direction until the uniaxial engineering strain $\varepsilon$ reaches $\pm 0.2$. In dynamic simulations, a Velocity Verlet algorithm is adopted with a time step of 2 fs and the NVT ensemble is used to keep a constant temperature of 10 K. The uniaxial engineering stress $\sigma$ is calculated following the virial stress formulation. Lattice defects are identified by the centrosymmetry parameter (CSP) [27].

## 3. Results and discussion

### 3.1. Tensile loading

Stress-strain curves of the nanotwinned nanotubes with different TB spacing $\lambda$ and wall thickness $t$ under tensile loading are given in Fig. 2 (a–b); corresponding strengths $\sigma_Y$, which correlates with dislocation initiation or crack formation, are presented in Fig. 2(c) as a function of $\lambda$ and $t$. Compared with their single crystalline counterparts, nanotwinned nanotubes have a lower tensile strength. For the same $\lambda$, $\sigma_Y$ is nearly independent of $t$ when $t > 2$ nm but positively correlates with $t$ when $t \leq 2$ nm.

Atomic structures of the nanotubes with different wall thickness $t$ on the threshold of yielding/failure under tensile loading are presented in Fig. 3, for the cases of single crystalline nanotubes, as well as nanotwinned nanotubes with $\lambda = 35.23$ nm and $\lambda = 3.06$ nm, respectively. In single crystalline nanotubes, dislocations on distant {110} slip planes are nucleated on both inner and outer surfaces, regardless of the wall thickness $t$. For the nanotwinned nanotubes, when $t = 12$ nm, dislocations on distant {110} slip planes are nucleated from the intersections between the TB and the inner/outer surfaces; when $\lambda$ is small, these dislocations interact with TBs and are transmitted across them (Fig. 3(e)), in consistent with previous MD simulations of interactions between single edge/screw dislocation and a TB in BCC W [28,29]. Clearly, with a decreasing $\lambda$, there exists a larger number of TB/surface intersection sites that are prone to nucleate more dislocations; as a

consequence, when $t > 2$ nm, $\sigma_Y$ decreases with a decreasing $\lambda$. We remark that, unlike the previous experimental and MD work of tensile loading of nanotwinned nanopillars in Cu which exhibited a critical $\lambda$ for ductile-brittle transition [30], no such transition is found in our work. When $t \leq 2$ nm, the nanotwinned nanotubes fail in a brittle manner, i.e., cracks are formed along the TBs in the absence of dislocation nucleation, as depicted in Fig. 3(d) and (f). Because neither TBs nor cracks have a size-dependent stress field, the strength $\sigma_Y$ becomes nearly invariant with $\lambda$ when $t \leq 2$ nm, as shown in Fig. 2(c).

### 3.2. Compressive loading

Stress-strain curves of nanotwinned nanotubes with different TB spacing $\lambda$ and wall thickness $t$ under compressive loading are given in Fig. 4(a–b). For those curves with two major "peaks", the threshold of yielding/failure, at which point the uniaxial engineering stress is considered the strength, is defined as initiation of dislocations or buckling near the second "peak" because the first "peak" corresponds to the formation of the twinning-like {334} planar defects which disappear at higher strains [20]. Similar to the case of tensile loading, (i) for the same $\lambda$, the strength $\sigma_Y$ decreases with a smaller $t$ when $t \leq 2$ nm but is almost independent of $t$ when $t > 2$ nm, as shown in Fig. 4(c); (ii) for the same $t$, the nanotwinned nanotubes have a lower strength than their single crystalline counterparts.

Atomic structures of nanotubes under compressive loading on the threshold of yielding/failure are presented in Fig. 5, for the cases of single crystalline nanotubes, as well as nanotwinned nanotubes with $\lambda = 35.23$ nm and $\lambda = 3.06$ nm, respectively. In single crystalline nanotubes, dislocations on adjacent {110} slip planes are formed at both inner and outer surfaces regardless of the wall thickness $t$. For nanotwinned nanotubes, when $t = 12$ nm, the lattice in each grain, be it twin or matrix, is first rotated to accommodate the compressive loading, before dislocations on adjacent {110} slip planes are nucleated from the intersections between the TBs and the inner/outer surfaces, as shown in Fig. 5(c) and (e). When $\lambda$ is small, these dislocations interact with the TBs and are transmitted across them (Fig. 5(e)). In contrary to the case of tensile loading, for the same $t$, the nanotubes with a smaller $\lambda$

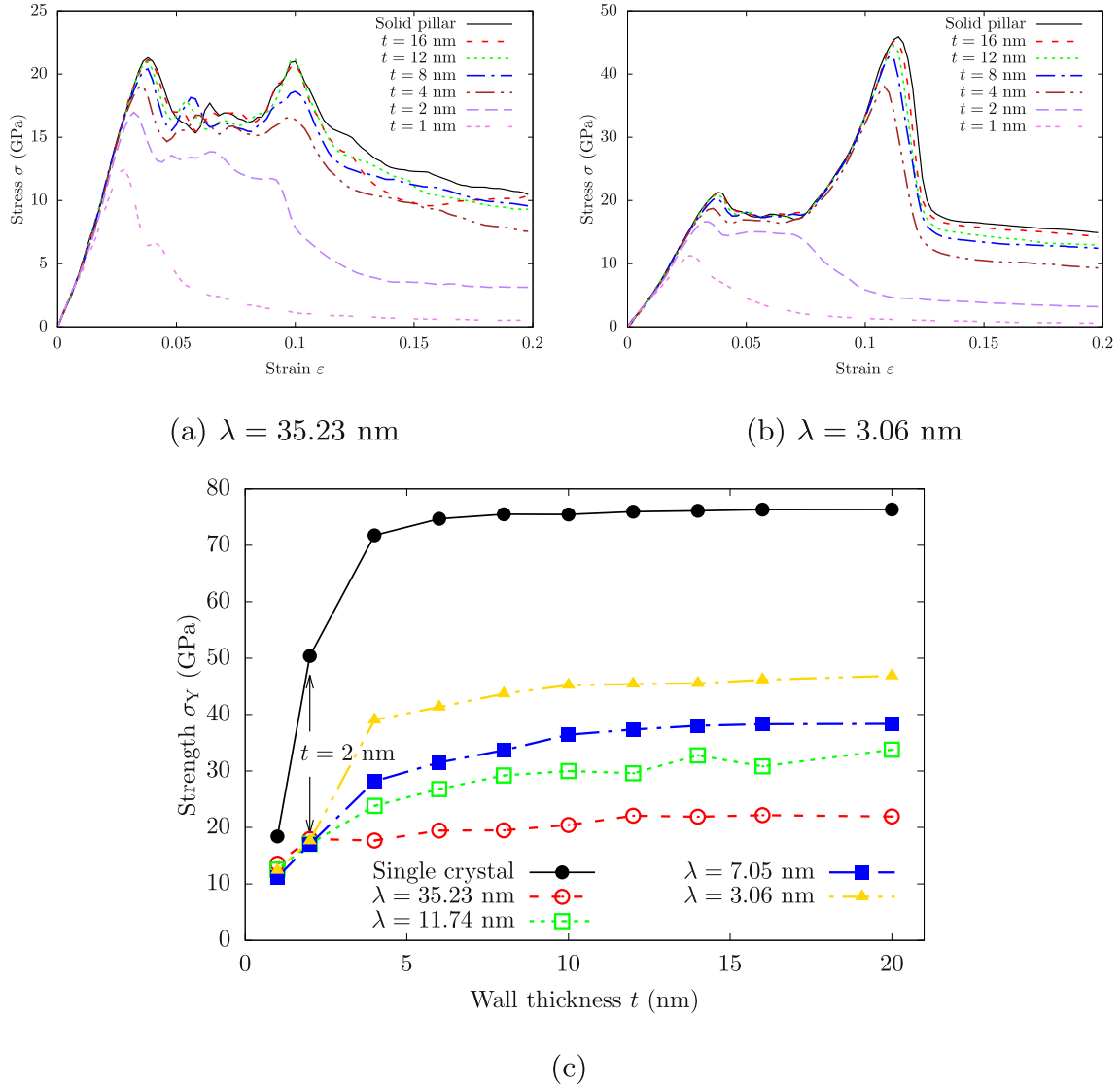


**Fig. 4.** Stress-strain curves of the nanotwinned nanotubes under compressive loading with different wall thickness $t$ when TB spacing (a) $\lambda = 35.23$ nm and (b) $\lambda = 3.06$ nm. The strength $\sigma_Y$ as a function of $t$ and $\lambda$ is given in (c). Note that the cases of solid nanopillars ($t = R = 20$ nm) and single crystalline nanotubes are also presented as references.

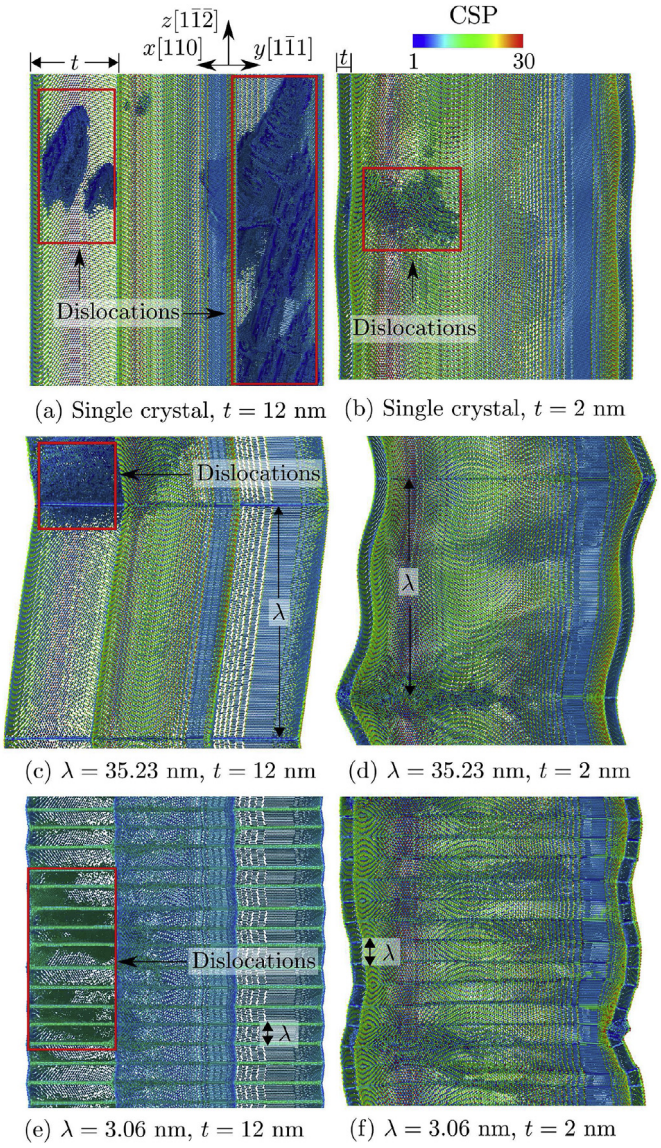


**Fig. 5.** Under compressive loading, snapshots of atomic structures on the threshold of yielding/failure in single crystalline nanotubes with wall thickness (a) $t = 12$ nm and (b) $t = 2$ nm, nanotwinned nanotubes ($\lambda = 35.12$ nm) with (c) $t = 12$ nm and (d) $t = 2$ nm, as well as nanotwinned nanotubes ($\lambda = 3.06$ nm) with (e) $t = 12$ nm and (f) $t = 2$ nm. Atoms are colored by CSP [27]; those with a CSP smaller than 1 are removed.

have a higher strength $\sigma_Y$ under compressive loading. This tension-compression asymmetry can be attributed to the different plastic deformation mechanisms: dislocations on distant slip planes in tensile loading but on adjacent slip planes in compressive loading. We remark that this finding is consistent with an earlier study of nanotwinned solid nanopillars in W [20] but not with that in Fe [19].

When $t \leq 2$ nm, the nanotubes fail by buckling, similar to the solid nanopillars with a large length-to-diameter aspect ratio [31–34]. The buckling of the nanotubes is also reflected in the stress-strain responses: (i) the stress-strain curves for $t \leq 2$ nm, which have only one major "peak", differ significantly from those with a larger $t$, as shown in Fig. 4(a–b), (ii) given the absence of the size effect of the buckling, the strength $\sigma_Y$ is approximately the same for different $\lambda$, as shown in Fig. 4(c). We remark that only local buckling, but not global buckling, is observed in all our simulations.

### 3.3. Strain rate effects

In this section, we perform MD simulations to demonstrate how the strain rate $\dot{\varepsilon}$ affects the deformation of the nanotwinned nanotubes when $\lambda = 35.23$ nm and 3.06 nm, respectively. To this end, apart from the strain rate of $\pm 10^9$ s$^{-1}$, two lower strain rates — $\pm 5 \times 10^8$ s$^{-1}$ and $\pm 2 \times 10^8$ s$^{-1}$ — are employed for both tensile and compressive loading; molecular static simulations using the conjugate gradient algorithm with an incremental engineering strain $\pm 0.001$ at each loading step are also conducted for comparison. As can be seen in Fig. 6, the stress-strain responses of the nanotubes vary with $\dot{\varepsilon}$. In specific, a higher strain rate results in a higher strength $\sigma_Y$ when $t > 2$ nm, as shown in Fig. 7. However, the strain rate effects become negligible when $t \leq 2$ nm. It appears that under compressive loading, the nanotubes with the same $\lambda$ and $t$ are more sensitive to the variation of $\dot{\varepsilon}$ than under tensile loading. In both tension and compression, for the same $t$, the strain rate effect becomes more pronounced when $\lambda$ is smaller. In particular, the single crystalline nanotube under tensile loading is somewhat independent of $\dot{\varepsilon}$, while the strength of the nanotwinned nanotube ($\lambda = 3.06$ nm) under compressive loading at $10^9$ s$^{-1}$ is more than twice that at $2 \times 10^8$ s$^{-1}$. Further analyses of the atomic structure on the threshold of plasticity/failure (Fig. 8) confirm that the patterns of dislocation nucleation, crack formation, and buckling are similar for the three strain rates examined in this paper, i.e., (i) under tensile loading, the nanotwinned nanotubes yield by dislocation nucleation on distant slip planes when $t$ is large but fail by crack formation when $t$ is small, (ii) under compressive loading, the nanotwinned nanotubes yield by dislocation nucleation on adjacent slip planes when $t$ is large but fail by buckling when $t$ is small. We remark that while a higher strain rate results in a higher local stress [35] which alters the stress-strain response, the strain rates employed in our simulations are not high enough to initiate deformation twinning [36], so the plastic deformation is dominated by dislocation slip at all rates.

## 4. Conclusions

In this paper, large-scale MD simulations are conducted to investigate tensile and compressive uniaxial deformation of the nanotwinned nanotubes in BCC W. Solid nanopillars without the interior hollow and/or nanotubes without the nanoscale twins are also explored as references. To our best knowledge, this work is the first attempt in the literature to shed new light on low dimensional nanoscale metallic structures containing both nanoscale twins and cylindrical hollow. In this regard, our work may serve as a precursor to more computational and experimental work in this topic, which may be possible thanks to a recently developed experimental technique that can grow nanoscale twins in metallic materials with high stacking fault energy [37]. The following key conclusions can be drawn from the observations reported and discussed in this paper:

1. Under both tensile and compressive loading, (i) the nanotubes exhibit a lower strength than their solid nanopillar counterpart, regardless of whether the nanoscale twins are introduced, (ii) the twinned structures exhibit a lower strength than their twin free counterparts, regardless of the wall thickness $t$. In other words, in BCC W, strength of nanopillars cannot benefit from their nanotwinned or hollowed structure, in contrary to FCC metallic materials [2–9,30];
2. With the same TB spacing $\lambda$, the strength of the nanotubes under tensile and compressive loading is nearly independent of the wall thickness $t$ when $t > 2$ nm (yielding by dislocation nucleation on distant {110} slip planes under tensile loading but on

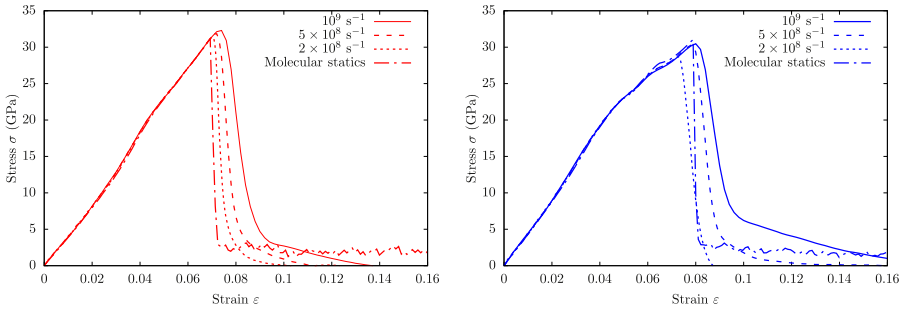


(a) $\lambda = 35.23$ nm, Tension (b) $\lambda = 3.06$ nm, Tension

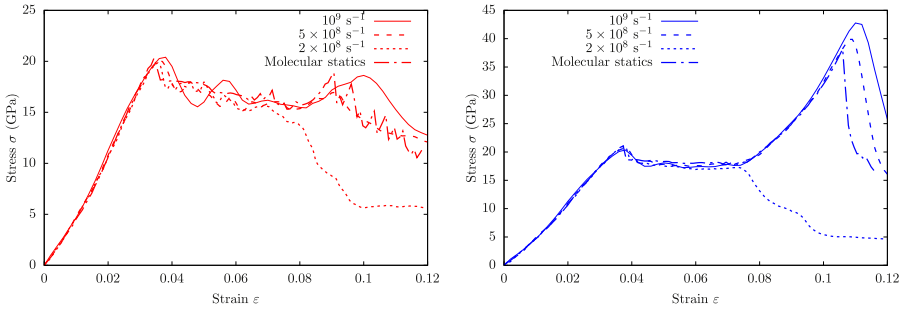


(c) $\lambda = 35.23$ nm, Compression (d) $\lambda = 3.06$ nm, Compression

**Fig. 6.** Stress-strain curves of the nanotwinned nanotubes with wall thickness $t = 8$ nm under (a–b) tension and (c–d) compression in cases of different TB spacing $\lambda$ and strain rate $\dot{\varepsilon}$. Molecular static simulation results are also shown for comparison.

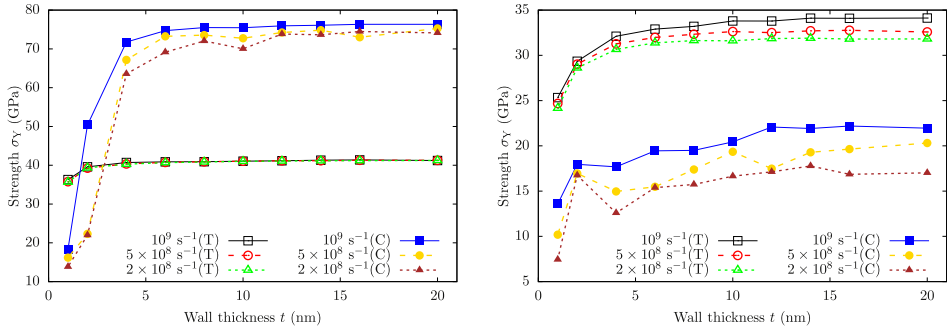


(a) Single crystal (b) $\lambda = 35.23$ nm

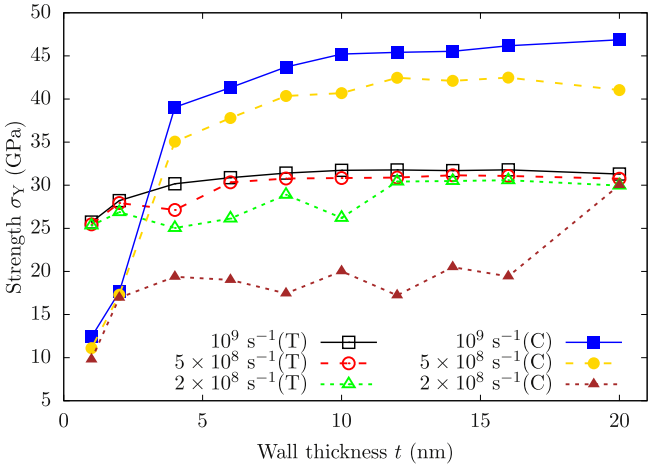


(c) $\lambda = 3.06$ nm

**Fig. 7.** The strength $\sigma_Y$ as a function of wall thickness $t$ and strain rate $\dot{\varepsilon}$ in the cases of (a) single crystalline nanotubes, (b) nanotwinned nanotubes with $\lambda = 35.23$ nm, and (c) nanotwinned nanotubes with $\lambda = 3.06$ nm.

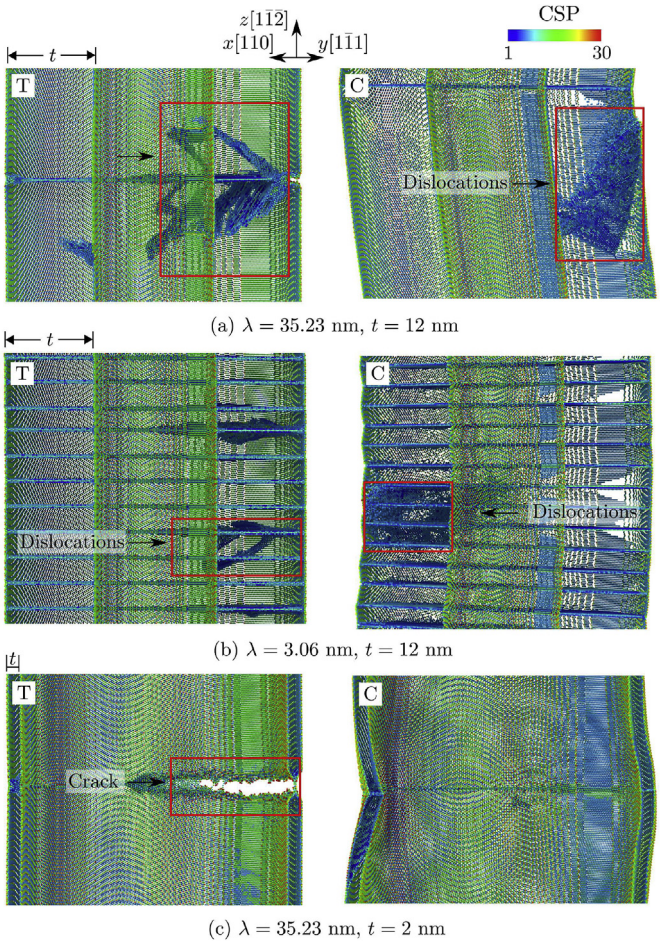


**Fig. 8.** Snapshots of atomic structures in nanotwinned nanotubes on the threshold of yielding/failure with (a) $\lambda = 35.12$ nm and $t = 12$ nm, (b) $\lambda = 3.06$ nm and $t = 12$ nm, as well as (c) $\lambda = 35.12$ nm and $t = 2$ nm, subject to tensile (left column, labeled by T) or compressive loading (right column, labeled by C). The strain rate $\dot{\varepsilon} = \pm 2 \times 10^8$ s$^{-1}$. Atoms are colored by CSP [27]; those with a CSP smaller than 1 are removed.

adjacent {110} slip planes under compressive loading) whereas it decreases with a smaller $t$ when $t \leq 2$ nm (failing by crack formation under tensile loading and buckling under compressive loading);

3. With the same $t(>2$ nm), a smaller $\lambda$ leads to a lower strength under tension but a higher strength under compression. This specific behavior can be attributed to their different plastic deformation mechanisms.
4. In all dynamic cases, a higher strain rate results in a higher yield strength. Moreover, the strain rate effect, which is more pronounced in compression than in tension, increases with a smaller $\lambda$.

## Acknowledgement

The work of SX was supported in part by the Elings Prize Fellowship in Science offered by the California NanoSystems Institute (CNSI) on the UC Santa Barbara campus. SX also acknowledges support from the Center for Scientific Computing from the CNSI, MRL: an NSF MRSEC (DMR-1121053). SZC would like to express his sincere gratitude for the financial support from the AVIC Center for Materials Characterisation, Processing and Modelling at Imperial College London. This work used the Extreme Science and Engineering Discovery Environment (XSEDE), which is supported by National Science Foundation grant number ACI-1053575.

## References

[1] J.R. Greer, J.T.M. De Hosson, Prog. Mater. Sci. 56 (2011) 654–724, https://doi.org/10.1016/j.pmatsci.2011.01.005. http://www.sciencedirect.com/science/article/pii/S0079642511000065.
[2] J.Y. Park, S. Im, Phys. Rev. B 77 (2008) 184109, https://doi.org/10.1103/PhysRevB.77.184109.
[3] M. Sun, F. Xiao, C. Deng, Appl. Phys. Lett. 103 (2013) 231911, https://doi.org/10.1063/1.4841995.
[4] E.P.M. Amorim, A.J.R. da Silva, E.Z. da Silva, J. Phys. Chem. C 112 (2008) 15241–15246, https://doi.org/10.1021/jp804345n.
[5] C. Ji, H.S. Park, Appl. Phys. Lett. 89 (2006) 181916, https://doi.org/10.1063/1.2372748.
[6] J. Zhang, C. Wang, R. Chowdhury, S. Adhikari, Appl. Phys. Lett. 101 (2012) 093109, https://doi.org/10.1063/1.4748975.
[7] C. Ji, H.S. Park, Nanotech 18 (2007) 115707, https://doi.org/10.1088/0957-4484/18/11/115707. http://stacks.iop.org/0957-4484/18/i=11/a=115707.
[8] R. Cao, Y. Deng, C. Deng, Acta Mater 86 (2015) 15–22, https://doi.org/10.1016/j.actamat.2014.11.053. http://www.sciencedirect.com/science/article/pii/S1359645414009069.
[9] L. Wang, C. Peng, J. Gong, Eur. J. Mech. A 28 (2009) 877–881, https://doi.org/10.1016/j.euromechsol.2009.01.002. http://www.sciencedirect.com/science/article/pii/S0997753809000035.
[10] Y. Mishin, M.J. Mehl, D.A. Papaconstantopoulos, A.F. Voter, J.D. Kress, Phys. Rev. B 63 (2001) 224106, https://doi.org/10.1103/PhysRevB.63.224106.
[11] M. Doyama, Y. Kogure, Comput. Mater. Sci. 14 (1999) 80–83, https://doi.org/10.1016/S0927-0256(98)00076-7. http://www.sciencedirect.com/science/article/pii/S0927025698000767.
[12] S.Z. Xu, Z.M. Hao, Q. Wan, IOP Conf. Ser. Mater. Sci. Eng. 10 (2010) 012175, https://doi.org/10.1088/1757-899X/10/1/012175. http://stacks.iop.org/1757-899X/10/i=1/a=012175.
[13] Y. Su, S. Xu, Mater. Sci. Eng. A 678 (2016) 153–164, https://doi.org/10.1016/j.msea.2016.09.091. http://www.sciencedirect.com/science/article/pii/S0921509316311741.
[14] S. Xu, Y. Su, D. Chen, L. Li, Mater. Lett. 193 (2017) 283–287, https://doi.org/10.1016/j.matlet.2017.02.005. http://www.sciencedirect.com/science/article/pii/S0167577X17301891.
[15] C. Deng, F. Sansoz, Nano Lett. 9 (2009) 1517–1522, https://doi.org/10.1021/nl803553b.
[16] C. Deng, F. Sansoz, Appl. Phys. Lett. 95 (2009) 091914, https://doi.org/10.1063/1.3222936.
[17] F. Hammami, Y. Kulkarni, J. Appl. Phys. 116 (2014) 033512, https://doi.org/10.1063/1.4890541.
[18] Y. Zhang, H. Huang, Nanoscale Res. Lett. 4 (2008) 34–38, https://doi.org/10.1007/s11671-008-9198-1. http://www.ncbi.nlm.nih.gov/pmc/articles/PMC2894070/.
[19] G. Sainath, B.K. Choudhary, Philos. Mag. 96 (2016) 3502–3523, https://doi.org/10.1080/14786435.2016.1240377.
[20] S. Xu, J.K. Startt, T.G. Payne, C.S. Deo, D.L. McDowell, J. Appl. Phys. 121 (2017) 175101, https://doi.org/10.1063/1.4982754.
[21] S. Plimpton, J. Comput. Phys. 117 (1995) 1–19, https://doi.org/10.1006/jcph.1995.1039. http://www.sciencedirect.com/science/article/pii/S002199918571039X.
[22] M.-C. Marinica, L. Ventelon, M.R. Gilbert, L. Proville, S.L. Dudarev, J. Marian, G. Bencteux, F. Willaime, J. Phys. Condens. Matter 25 (2013) 395502, https://doi.org/10.1088/0953-8984/25/39/395502. http://stacks.iop.org/0953-8984/25/i=39/a=395502.
[23] G. Bonny, D. Terentyev, A. Bakaev, P. Grigorev, D.V. Neck, Model. Simul. Mater. Sci. Eng. 22 (2014) 053001, https://doi.org/10.1088/0965-0393/22/5/053001. http://stacks.iop.org/0965-0393/22/i=5/a=053001.
[24] S.Z. Xu, Z.M. Hao, Y.Q. Su, Y. Yu, Q. Wan, W.J. Hu, Comput. Mater. Sci. 50 (2011) 2411–2421, https://doi.org/10.1016/j.commatsci.2011.03.019. http://www.sciencedirect.com/science/article/pii/S0927025611001625.
[25] S.Z. Xu, Z.M. Hao, Y.Q. Su, W.J. Hu, Y. Yu, Q. Wan, Radiat. Eff. Def. Solids 167 (2012) 12–25, https://doi.org/10.1080/10420150.2011.613393.
[26] S. Xu, Y. Su, Model. Simul. Mater. Sci. Eng. 24 (2016) 085015, https://doi.org/10.1088/0965-0393/24/8/085015. http://stacks.iop.org/0965-0393/24/i=8/a=085015.
[27] C.L. Kelchner, S.J. Plimpton, J.C. Hamilton, Phys. Rev. B 58 (1998) 11085–11088, https://doi.org/10.1103/PhysRevB.58.11085.
[28] Y. Cheng, M. Mrovec, P. Gumbsch, Philos. Mag. 88 (2008) 547–560, https://doi.org/10.1080/14786430801894577.
[29] M. Mrovec, C. Elsässer, P. Gumbsch, Philos. Mag. 89 (2009) 3179–3194, https://doi.org/10.1080/14786430903246346.
[30] D. Jang, X. Li, H. Gao, J.R. Greer, Nat. Nanotech. 7 (2012) 594–601, https://doi.org/10.1038/nnano.2012.116. http://www.nature.com/nnano/journal/v7/n9/full/nnano.2012.116.html.
[31] E. Rabkin, H.S. Nam, D.J. Srolovitz, Acta Mater 55 (2007) 2085–2099, https://doi.org/10.1016/j.actamat.2006.10.058. http://www.sciencedirect.com/science/article/pii/S1359645406008202.
[32] W. Jiang, R.C. Batra, Acta Mater 57 (2009) 4921–4932, https://doi.org/10.1016/j.actamat.2009.06.062. http://www.sciencedirect.com/science/

article/pii/S1359645409004212.
[33] P.A.T. Olsson, H.S. Park, Acta Mater 59 (2011) 3883–3894, https://doi.org/10.1016/j.actamat.2011.03.012. http://www.sciencedirect.com/science/article/pii/S1359645411001595.
[34] R.J. Milne, A.J. Lockwood, B.J. Inkson, J. Phys. D. Appl. Phys. 44 (2011) 485301, https://doi.org/10.1088/0022-3727/44/48/485301. http://iopscience.iop.org/0022-3727/44/48/485301.
[35] T. Zhu, J. Li, A. Samanta, A. Leach, K. Gall, Phys. Rev. Lett. 100 (2008) 025502, https://doi.org/10.1103/PhysRevLett.100.025502.
[36] R.E. Rudd, Philos. Mag. 89 (2009) 3133–3161, https://doi.org/10.1080/14786430903222529. http://www.tandfonline.com/doi/abs/10.1080/14786430903222529#preview.
[37] D. Bufford, Y. Liu, Y. Zhu, Z. Bi, Q.X. Jia, H. Wang, X. Zhang, Mater. Res. Lett. 1 (2013) 51–60, https://doi.org/10.1080/21663831.2012.761654.